

Journal of Materials Chemistry C

Accepted Manuscript



This article can be cited before page numbers have been issued, to do this please use: P. Prabakaran, S. Satapathy, P. Edamana and S. Sankararaman, *J. Mater. Chem. C*, 2017, DOI: 10.1039/C7TC04655C.



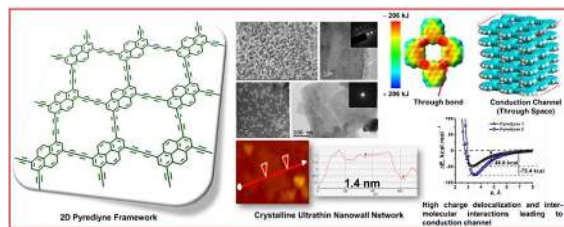
This is an Accepted Manuscript, which has been through the Royal Society of Chemistry peer review process and has been accepted for publication.

Accepted Manuscripts are published online shortly after acceptance, before technical editing, formatting and proof reading. Using this free service, authors can make their results available to the community, in citable form, before we publish the edited article. We will replace this Accepted Manuscript with the edited and formatted Advance Article as soon as it is available.

You can find more information about Accepted Manuscripts in the [author guidelines](#).

Please note that technical editing may introduce minor changes to the text and/or graphics, which may alter content. The journal's standard [Terms & Conditions](#) and the ethical guidelines, outlined in our [author and reviewer resource centre](#), still apply. In no event shall the Royal Society of Chemistry be held responsible for any errors or omissions in this Accepted Manuscript or any consequences arising from the use of any information it contains.

TABLE OF CONTENTS



Highly stabilized molecular interactions and bulk transport characteristics are achieved through the synthesis of ultrathin 2D nanowall network of pyridyne



Journal Name

ARTICLE

Architecting Pyrediyne Nanowalls with Improved Inter-Molecular Interactions, Electronic Features and Transport characteristics

Palani Prabakaran, Sitakanta Satapathy, Edamana Prasad^{*a} and Sethuraman Sankararaman^{*b}

Received 00th January 20xx,
Accepted 00th January 20xx

DOI: 10.1039/x0xx00000x

www.rsc.org/

Synthesizing graphdiyne analogues with a well-defined structure and desirable band gap is a challenging task. Herein, we present a novel, well-defined and highly structured crystalline π -conjugated nanowall framework, named as pyrediyne (pyrene+diyne=pyrediyne), with large in-plane periodicity. The bulk synthesis of the two-dimensional (2D) ultrathin polymeric framework of pyrediyne is achieved via a modified-Glaser-Hay coupling reaction using 1, 3, 6, 8-tetraethynylpyrene. The ultrathin π -conjugated crystalline pyrediyne nanowall is well characterized by Raman, SEM, AFM, HR-TEM and XPS techniques. Electronic structure information reveals the π -conjugated framework to be completely planar with C_s point group, where a tunable band gap of $E_g \sim 1.17$ eV can be achieved depending upon the number of pyrene units. The electrostatic potential maps reveals a complete π -delocalization of the electron cloud throughout the framework with high electronegative potential at the acetylenic linkages. This through-bond charge coupling via the conjugated network which in conjunction with the charge delocalization via π - π interactions in space accounts for the significant electrical conductivity $\{\sigma = 1.23(\pm 0.1) \times 10^{-3} \text{ S m}^{-1}\}$ in the organic material.

Introduction

Flat surfaces with high π -charge delocalization and high stability under harsh conditions makes 2D networks an extremely important building blocks for next generation devices.¹⁻⁷ In this context, there has been an increasing demand for carbon based nano structures with exotic physical and chemical properties, which resulted in the realization of carbon nanotubes,⁸⁻¹⁴ nanosheets,¹⁵⁻¹⁹ nanowalls²⁰⁻²³ and graphene.²⁴⁻³⁰ The latest entry in this series is graphdiyne, exhibiting potential towards diverse applications,³¹⁻³⁹ where the hexagonal benzene rings are connected by diacetylenic bonds.⁴⁰⁻⁴² However, the elusiveness of 2D nanosheet synthesis and their importance in transport applications still demands for the design and synthesis of novel carbon materials with well-defined structure and unique properties. Subtle design modifications in such flat π -systems could considerably alter optical and geometrical characteristics of the materials, leading to better charge transport properties.

Keeping in view the above facts, we plan to achieve a brand new type of carbon material of good synthetic scalability with much improved electronic features and transport abilities. The present work describes the successful attempt in synthesizing

an extremely flat, highly ordered pyrediyne (PDY) nanowall over Cu surface with much improved π -conjugation, delocalization features and better transport characteristics compared to that of graphdiyne. The present work also reports the bulk synthesis of pyrediyne, which involves a modified Glaser-Hay coupling reaction⁴¹ using 1,3,6,8-tetraethynylpyrene (TEP) as precursor. XPS, Raman and FT-IR studies were successfully used to characterize the molecular structure, while SEM, TEM, AFM and optical microscopy results substantiate the evidence towards formation of the ultrathin 2D framework. Remarkably, our synthetic strategy affords ultrathin and crystalline pyrediyne nanowall at room temperature with a well-defined domain structure and periodicity with narrow distributions of thickness (as thin as 1.4 nm) and lateral size (0.6 μm). We hypothesize the material to be transport active since the 1D potential energy surface calculations suggest (i) the possibility of high through-bond and through-space coupling interactions for binding, and (ii) a low band gap (E_g) of 1.17 eV, which is better than that of Si and comparable to that of graphdiyne.

Experimental

Materials

1,3,6,8-Tetraethynylpyrene (TEP) was synthesized according to reported procedure.⁴³ Acetone, Tetrahydrofuran (THF), tetra methyl ethylene diamine (TMEDA) were purchased from Spectrochem chemicals and used without further purification. Pyridine, phosphoric acid and nitric acid were purchased from Merck, India. Hydrochloric acid was purchased from Fisher

^a Prof. Edamana Prasad, Department of chemistry
Indian Institute of Technology Madras, Chennai 600036 (India)
E-mail: pre@iitm.ac.in

^b Prof. Sethuraman Sankararaman, Department of chemistry
Indian Institute of Technology Madras, Chennai 600036 (India)
E-mail: sankas@iitm.ac.in

Electronic Supplementary Information (ESI) available: See
DOI: 10.1039/x0xx00000x

ARTICLE

Journal Name

Scientific chemicals. Copper plate and copper powder were purchased from S.D. fine chemicals, Chennai, India.

Pyrediyne Nanowalls Synthesis

Copper plates (2 × 2 cm) were ultrasonically cleaned with phosphoric acid, 1M HCl, water and acetone to make surface smoother. Washed copper plates were dried under the flow of N₂. Copper plates were placed in the mixed solution of acetone (50 mL), pyridine (2.5 mL), and tetra methyl ethylene diamine (TMEDA) (0.5 mL). TEP (20 mg) was dissolved in 200 mL of acetone and the solution was added drop wise into the reaction mixture as mentioned above. Then the mixture was warmed at 50 °C under N₂ atmosphere for 1 day. The reaction flask was covered by Al foil and protected from light. Finally, the copper plates were washed with acetone and THF to remove unreacted TEP followed by drying under nitrogen. Nanowalls grown over copper plates were further taken for characterization.

Bulk Synthesis of Pyrediyne Powder

After successful synthesis of pyrediyne (PDY) nanowalls, we have utilized 1,3,6,8-tetraethynylpyrene to synthesize the PDY powder in bulk. Copper powder (400 mg) was added in the mixed solution of acetone (100 mL), pyridine (5 mL), and tetra methyl ethylene diamine (TMEDA) (1 mL). TEP (40 mg) was dissolved in 400 mL of acetone and added into the reaction mixture as mentioned above. Then the reaction mixture was constantly stirred at 50 °C under a N₂ atmosphere for 2 days. The reaction flask was covered by Al foil to protect from light. After completion of the reaction, the crude product was filtered and washed with acetone and water to remove pyridine and TMEDA. The washed crude product was added slowly to 20 mL of concentration nitric acid (18 M) to remove the copper powder. This was followed by dilution with water and subsequent filtration to form the pure product (~38 mg).

Techniques

The morphology of pyrediyne nanowalls were examined using scanning electron microscopy (SEM) (FEI quanta FEG 400 at 5 kV). Smaller quantities of nanowalls were grown over the copper plate and then directly carried out for the SEM analysis. Aqueous dispersion of nanowalls was drop casted over silicon wafer (111) for SEM (Inspect F at 20 kV) imaging. The as prepared samples were kept under vacuum desiccator for 24 hours for drying. All of the sample gold sputter coated 30 s and then imaged under SEM. The morphology analysis of the pyrediyne was done using transmission electron microscopy (TEM) (JEOL JEM-2000 at 200 kV). For TEM, water dispersed pyrediyne solution was drop casted on carbon coated copper grid (200 mesh) and kept for drying for 24 hours under vacuum. A similar sample preparation procedure over glass substrate was employed for OM studies using optical microscope (Nikon Eclipse LV 100 POL). AFM studies experiments were performed using Park systems XE 100 and the height image analysis was carried out using XEI imaging software. Raman spectra were collected using MultiRAM FT-Raman spectrometer (Germanium detector with the resolution

of 4 cm⁻¹). Powder-XRD patterns of pyrediyne were recorded using Bruker D8 Advance X-ray diffractometer using Cu-K_α radiation (λ=1.54 Å). UV spectra were recorded using JASCO V-660 spectrophotometer. IR spectrum was recorded using JASCO FT/IR-4100 spectrometer. X-ray photoelectron spectroscopy (XPS) measurements was carried out using Omicron ESCA probe spectrometer with polychromatic Mg K_α X-rays (hν = 1253.6 eV).

Conductivity Measurement

Impedance spectroscopy of the solid powder was recorded using Bio-Logic SP-150 instrument at 25 °C over the frequency range from 100 kHz to 10 mHz with an AC perturbation of 10 mV at the 0V DC level. The solid powder was made into pellet of area (a = 1.2474 cm²) using a hydraulic press and was then placed in a cylindrical cell having two stainless steel (electrodes) stoppers at both ends. The Nyquist plot semicircle was then fitted to obtain the resistance value using the Z-view software (Version 3.2c, EC lab) of the instrument. The electrical conductivity was calculated using the following equation.

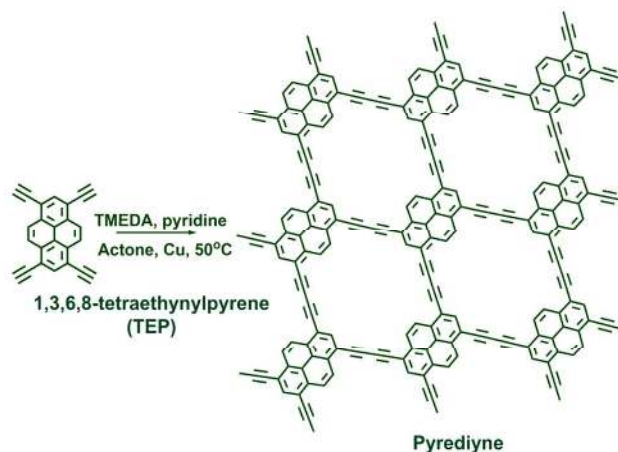
$$\sigma = \frac{l}{R \times a}$$

where, 'l' is the thickness, 'R' is the resistance and 'a' is the area of the solid pellet. The experiment was repeated three times and the average of all the resistance value is considered for the above equation.

Results and discussion

Synthesis and Molecular Symmetry of Highly Planar Pyrediyne Nanowalls

The schematic illustration of the synthesis process of pyrediyne nanowall (scheme 1), DFT optimized molecular geometry with energy and point group symmetry is depicted in figure 1. The π-conjugated 2D framework is fully flat and highly planar as a result of Cs point group symmetry.⁴⁴



Scheme 1. Synthetic scheme with the molecular structure of 1,3,6,8-tetraethynylpyrene (TEP) and pyrediyne.

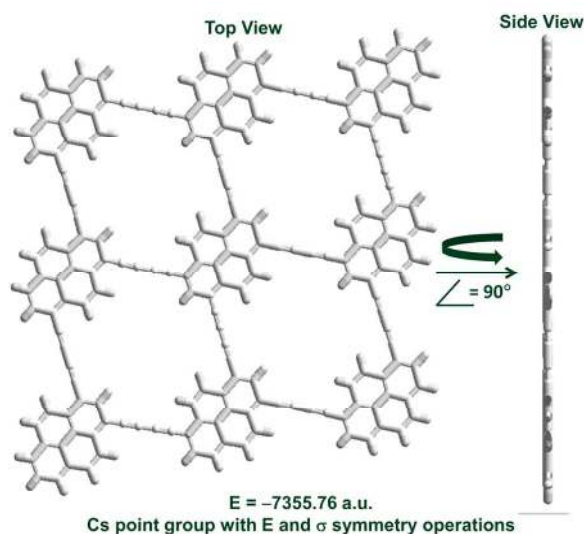


Figure 1. Grimme's dispersion corrected⁴⁵ B3LYP-D/6-31G (d) optimized geometry, energy and point group symmetry of pyrediyne are shown (Top and side views).

The synthesis of the pyrediyne was carried out using copper as catalyst. Copper powder was used for the bulk synthesis of pyrediyne. It has been observed that polymeric 2D nanowall framework of pyrediyne can be developed upon replacing copper powder by copper plates. Briefly, Copper plates were placed in a solution of acetone (50 mL), pyridine (2.5 mL), and tetra methyl ethylene diamine (TMEDA) (0.5 mL). 1,3,6,8-Tetraethynylpyrene TEP (20 mg) was dissolved in 200 mL of acetone and the solution was added drop wise into the reaction mixture. Copper gets easily converts to Cu^{2+} ions in the presence of a catalytic amount of base, where a Glaser–Hay reaction can take place efficiently with the aid of TMEDA (See Experimental Section for Details).

Microscopic Observation of Multilayer Pyrediyne Growth and Its Reproducibility

It was observed that the reaction was stopped upon the formation of a few multilayers on the Cu surface. Since most of the reactants are still present in the reaction mixture, reusing the reaction mixture resulted in the formation of the nanowalls over the newly added copper plates. Figure 2a shows the scanning electron microscope (SEM) image of pyrediyne nanowalls on the copper plate.

It can be seen that the π -stacked sheets were sufficiently transparent and freestanding to traverse the holes in the carbon matrix. The pyrediyne nanowalls on copper foil with the element content mapping are given in the supporting information (Figure S1). The cyan colored particles indicate copper (Cu), while the red ones accounts for the uniform distribution of carbon (C) throughout the π -conjugated framework. The intact growth of the nanowalls is further characterized by SEM experiments as shown in Figure 2b-d, which also accounts for the high reproducibility of the method used in the case.

Figure 3 shows the multilayered structure of pyrediyne from scanning electron microscopy (SEM), atomic force microscopy (AFM) {on Si(111) wafer} and optical microscopy

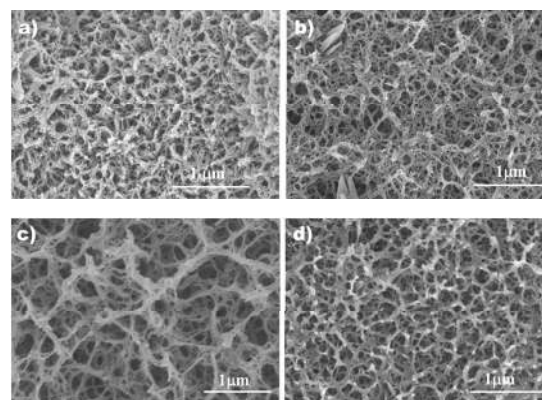


Figure 2. SEM images recorded over the Cu surface accounting for the growth of the 2D pyrediyne nanowalls from the reaction mixture after a) 1st cycle b) 2nd cycle, c) 3rd cycle and d) 4th cycle. The reaction mixture was re-used four times, and each time, a new Cu plate was used.

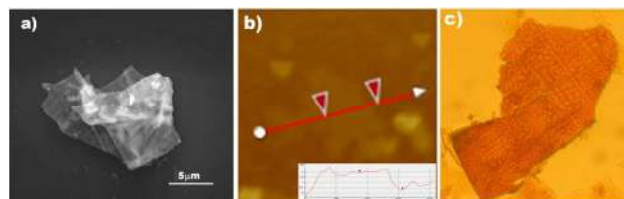


Figure 3. a) SEM, b) AFM image (semi-contact mode) studies on Si(111) wafer and c) OM image of the transparent 2D nanowall recorded over glass substrate.

(OM) {over glass substrate} studies. The SEM image in Figure 3a indicates the layered structure of the transparent nanowalls, π -stacked over one another. The ultrathin layered 2D framework of pyrediyne exclusively composed of carbon material is then characterized from the energy dispersive x-ray spectrometry (EDS) which confirmed the carbon content along with a few peaks vouching for the silicon and oxygen content arising from silicon substrate Si(111) used to record the SEM image (Figure S2, Supporting Information). The AFM image in Figure 3b further confirmed the sheet morphology of height 1.4 ± 0.3 nm with lateral size of 600 ± 35 nm. Optical microscopy image also confirms the sheet morphology of pyrediyne, vide Figure 3c.

2D Periodicity and High Crystallinity of Multilayered Pyrediyne

Figure 4 shows the transmission electron microscopy (TEM) studies which are consistent with the other microscopic results. Figure 4a shows TEM images of transparent π -stacked pyrediyne nanowalls. A typical low-magnification TEM image of the π -stacked pyrediyne nanowalls, separated by a distance of 0.48 nm, is given in Figure 4b. The selected area electron diffraction (SAED) image followed by TEM, confirmed the highly ordered in-plane periodicity and crystallinity of the well-defined ultrathin 2D lattice framework of pyrediyne.

ARTICLE

Journal Name

High-resolution TEM (Figure 4b) showed lattice fringes with an interval of 0.48 nm, which was further confirmed by XRD (figure 7). In the SAED assignment, we also accounted for the (222), (521), and (400) reflections accounting for the body centred cubic (BCC) lattice structure of the crystalline

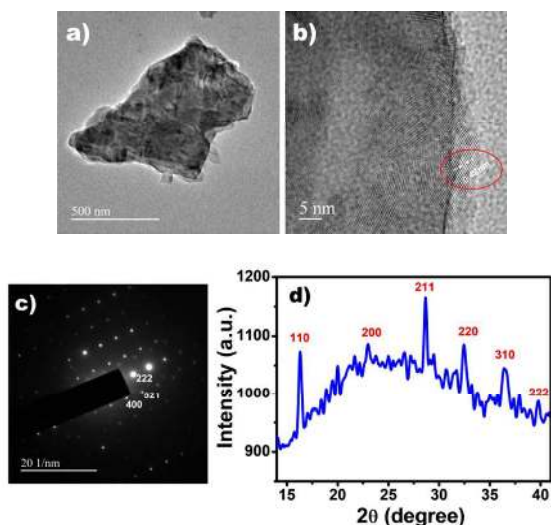


Figure 4. HR-TEM images of a) π -stacked sheets of pyrediyne nanowall, b) lattice fringe spacing (red encircled) between the nanowalls, c) SAED pattern and d) XRD results from the pyrediyne nanowall.

pyrediyne. Further evidence suggesting high crystallinity for the material has come from the appearance of several sharp peaks in the x-ray diffraction pattern as shown in Figure 4d. The calculated d values of 5.42, 3.85, 3.11, 2.75, 2.46, 2.26 Å from the XRD results correspond to (110), (200), (211), (220), (310), and (222) reflections of a BCC lattice for the pyrediyne nanowall along with high periodicity along with the lattice parameter of $a=7.7$ Å.

The Diacetylenic Linkage/The Carbon-Carbon Bond (sp^2 - $(sp-sp)_2$ - sp^2)

Raman spectra of pyrediyne in Figure 5 indicates two weak bands at 460 and 614 cm^{-1} and six strong bands positioned around 1240, 1364, 1604, 1986, 2125 and 2195 cm^{-1} . The band at 460, 614, 1240, 1364 and 1604 cm^{-1} indicate the presence of pyrene.⁴⁶⁻⁴⁹ The 460 and 614 cm^{-1} bands are assigned to the stretching vibrations arising from the pyrene skeleton. The band at 1240 cm^{-1} is due to the CH in-plane bending, while the strong band at 1364 cm^{-1} is from the C-C stretching coupled with weak ring-breathing vibrations. The peak at 1604 cm^{-1} is the characteristic band for the C-C stretching vibration. 1,3,6,8-tetraethynylpyrene (TEP) shows sharp peaks around 2100 cm^{-1} that could be due to the carbon-carbon triple bond stretching. The band underwent a hypochromic shift to 2125 cm^{-1} upon reaction with a diyne linkage.⁴¹ This hypochromic shift suggests the formation of acetylenic linkages ($-C\equiv C-C\equiv C-$) architecting the 2D nano network as shown in Figure 5. From Raman spectra, we conclude that the pyrene moieties in the nanowall are tethered with diacetylenic linkages.

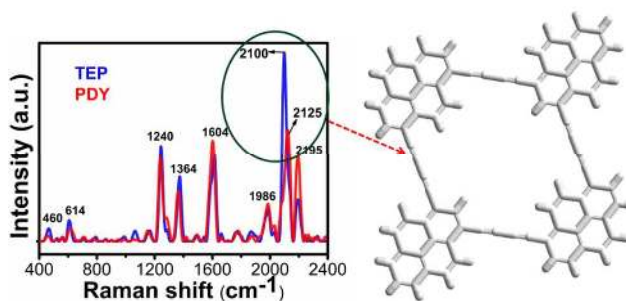


Figure 5. Raman spectra vibration peaks from pyrediyne confirming the acetylenic linkage connecting the pyrene network.

Bulk Pyrediyne; Morphology and Microarchitectures

Copper plates were used to synthesize the nanowalls while copper powder was used to synthesize bulk pyrediyne in powder form (See Experimental Section for Synthetic Procedure Details) with high scalability. Figure 6 shows the electron microscopy studies for bulk pyrediyne. The size data was evaluated from 106 independent nanodomains, where the average size of the flakes varied from 60-200 nm, as shown in Figure 6c. The average size of the flakes were found to be 120 ± 10 nm. The pyrediyne powder characterized from the energy dispersive x-ray spectrometry (EDS) which confirmed the carbon content along with a few peaks vouching for the indium, tin and oxygen content arising from indium tin oxide (ITO) glass used to record the SEM image (Figure S3, Supporting Information). Bulk Pyrediyne is further characterized by TEM which revealed the layered sheet nature of the nanowall as shown in Figure 6d. The selected-area diffraction pattern (SAED) indicates the semi crystalline nature with lesser number of diffraction spots as shown in Figure 6e.

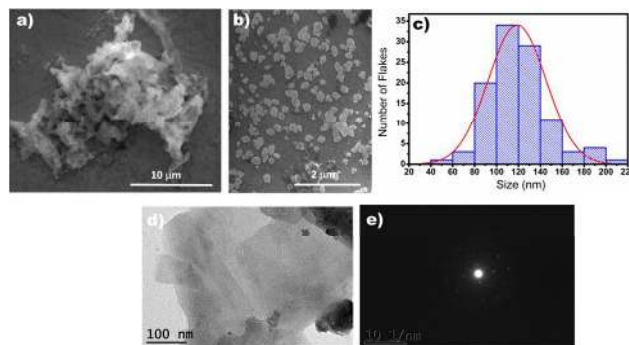


Figure 6. SEM images of bulk pyrediyne at a) low and b) high magnification, c) Size distribution and its Gaussian fitting (red line). (A total of 106 independent flakes were considered for averaging), d) High resolution TEM micrograph confirming the nanosheet structure and e) selected area diffraction (SAED) image from the pyrediyne nanosheet.

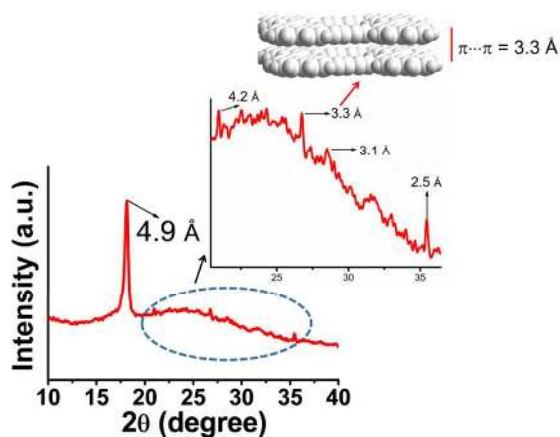


Figure 7. Powder X-ray diffraction pattern from the bulk pyrediyne.

Figure 7 shows the powder x-ray diffraction results, recorded from the bulk pyrediyne. As evident, the peak intensities for bulk pyrediyne are relatively lesser (zoomed view, Figure 7) as compared to the previously observed intensities for the nanowalls, accounting for a relatively lesser crystallinity. This is also evident from lesser spots in the corresponding SAED image for the bulk pyrediyne (Figure 6e). The diffraction peak at $2\theta = 26.75^\circ$, indicates an interlayer $\pi \cdots \pi$ spacing of 0.33 nm.

Thermogravimetric analysis (TGA) was performed to understand the thermal stability of the newly synthesized pyrediyne (Figure S4, Supporting Information). In the derivative plot, we have found two major peaks at 345.55 °C and 584.04 °C. Among the two step degradation process, the 1st peak at 345.55 °C was assigned to the degradation of the terminal ethynyl pyrene units in the nano-sheet, whereas the 2nd peak at 584 °C was due to the degradation of the 2D polymeric framework. Minor contributions at 220 °C can be assigned to the release of moisture content.

In bulk synthesis of pyrediyne, concentrated nitric acid was used to remove the copper powder from the reaction mixture. FT-IR spectra for the pyrediyne nanowalls and pyrediyne powder recorded after washing with nitric acid (Figure S5, Supporting Information). The intactness of almost all the stretching vibrations confirms its high chemical stability, where the structural integrity remains unaffected in response to strong oxidizing agents, i.e., conc. HNO_3 .

Uniform Chemical Composition and Bonding

In addition, the elementary composition and bonding structure is studied systemically using high-resolution X-ray photoelectron spectroscopy (XPS), in order to discern the chemical environment of each element involved in the formation of pyrediyne nanowall network, vide Figure 8. The spectra of XPS indicate that the pyrediyne nanowalls were mainly composed of elemental carbon, which was identical to the result of energy-dispersive spectrometry (EDS) (Figure S3, Supporting Information).

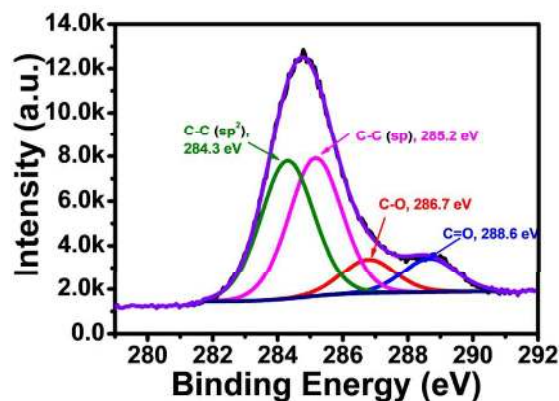


Figure 8. XPS spectra for the pyrediyne nanowalls deconvoluted for C 1s.

Moreover, carbon was distributed uniformly across the whole sheet, indicating the uniform chemical composition of the sheet. X-ray photoelectron spectroscopy (XPS) shows C 1s binding energy profile of pyrediyne (Figure 8). The peak at 285.2 eV showed essentially identical binding energy for the C 1s orbital. In detail, C 1s peak can be deconvoluted into four sub-peaks with major contributions from $\text{C}\equiv\text{C}$ and $\text{C}=\text{C}$ species. The abundance ratio of the sp/sp^2 carbons was 1.03, which was in quite good agreement with the chemical composition of pyrediyne. No copper trace was detected therein, which was also confirmed by high-resolution XPS focusing on the Cu 2p region (Figure S6, Supporting Information). The first peak at 248.3 eV corresponds to sp^2 hybridization while the second peak at 285.2 eV corresponds to sp hybridization of pyrediyne.^{50,51} Hybridization of sp and sp^2 confirms that the well-defined 2D structure of pyrediyne nanowall network was composed of pyrene linked with two acetylenic linkages. Minor contributions to the C 1s envelope was ascribed to C–O and C=O species at 286.7 eV and 288.6 eV, respectively. The calculated oxygen/carbon ratio was very minute, i.e., 0.3 and their presence might be due to the adsorption of O_2 when pyrediyne was exposed to air.⁴²

Electronic Structure and Density of States

Since, pyrediyne is a newly constructed nanowall network, it becomes utmost important to shed light on its electronic structure which can be correlated with its potential to depict transport abilities in organic electronics. Figure 9a depicts the DFT computed electrostatic potential surface (ESP maps) of pyrediyne which infers high delocalization of π -electron cloud throughout the conjugated 2D framework.

The careful analysis of the ESP maps further gives us a clear picture of high delocalization of the electron densities at the diacetylenic linkages as compared to the peripheral pyrene surfaces. This confirms the significantly high coupling of charge densities through bond along the acetylenic linkages that connects the peripheral pyrenes.

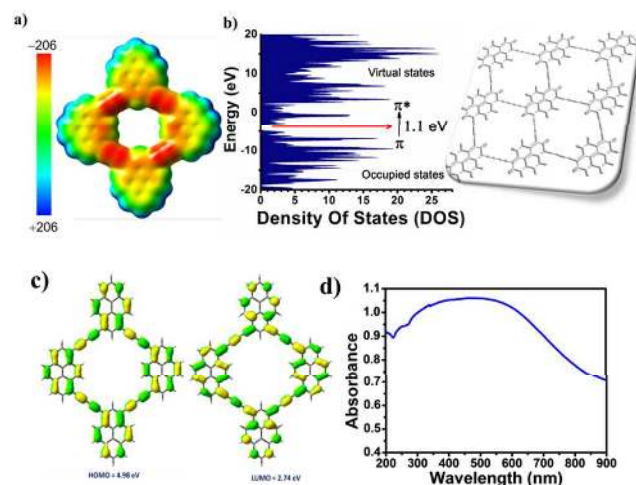


Figure 9. a) Electrostatic potential map (Grimme's dispersion corrected B3LYP-D/6-31G(d)) depicting the highly π -rich aromatic acetylenic linkages w.r.t that of the pyrene surfaces. The red and the blue part on the scale denote the electronegative and electropositive potentials. (isovalence = 0.002), b) The density of states (DOS) for the highly delocalized optimized geometry of single pyrediylene nanowall as shown in the box, c) The HOMO and LUMO isodensity surfaces and d) the solid state UV-Visible absorption spectra for the fine powder of pyrediylene.

The density of states (DOS) calculations, as shown in Figure 9b further accounts for a reasonable direct band gap of $E_g = 1.17$ eV. This is an advantage over the indirect band gap of Si ($E_g = 1.29$ eV) and is also comparable to the theoretical band gap of graphdiyne ($E_g = 1.1$ eV),⁵²⁻⁵⁵ employing similar level of theory. From Figure 9b, it can be seen that the densities of the virtual and the occupied states are much high due to high delocalization of π electron cloud throughout the network and further the densities of the virtual states are much higher as compared to that of the occupied states, which provides a much better pathway for tunneling of charge within the two states.

The enhanced coulomb interactions in reduced dimensionality^{44,45} mainly affect the E_g as the columbic force of attraction for a quassiparticle (electron-hole pair) which is mainly given by,

$$E_c = -\frac{e^2}{4\pi\epsilon\epsilon_0 r}$$

Where, E_c is the columbic force, e is the electron charge ϵ is the dielectric constant and r is the exciton radius.

Hence we went on to compare the DOS of two different pyrediynes on the basis of number of pyrene rings (Figure S7, Supporting Information). The E_g value for the framework with 9 pyrene rings is 1.17 eV while for the one with 4 pyrene rings is 1.52 eV, estimated by using the same level of theory (B3LYP-D/6-31G(d)). Clearly the DOS became much improved in the network with more number of pyrene rings due to high delocalization and π -conjugation. Hence, we suggest that the direct band gap of pyrediylene network with pyrenes as the core is a much improved one compared to that of graphdiyne with relatively less delocalized benzene rings as cores. Figure 9c depicts the HOMO and LUMO isodensity surfaces of pyrediylene

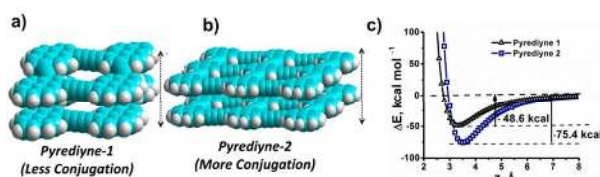


Figure 10. The MM+ optimized π -stacked dimers of pyrediynes with a) lesser conjugation (Pyrediylene-1), b) increased conjugation (Pyrediylene-2) and c) conjugation dependent molecular interaction energies /1D potential surface of the corresponding pyrediylene dimers. $\Delta E = \{E(\text{bound dimer}) - 2 \times E(\text{monomers})\}$.

which shows uniform distribution of electron densities over the 2D framework due to high conjugation and hence validates the broad UV-spectrum covering the entire UV-Vis range from 300-900 nm, vide Figure 9d.

Improved Inter-Molecular Interactions in Pyrediylene

In order to account quantitatively for the molecular interactions providing additional stability to the pyrediylene nanowalls, we computed the interaction energy profiles (potential energy curves) for both the pyrediylene dimers using molecular mechanics simulations (MM+)⁵⁶, vide Figure 10. The MM+ optimized pyrediylene dimers are bound via $\pi \cdots \pi$ interactions as shown in Figure 10a and Figure 10b. The potential energy curves are obtained by plotting the interactions energies obtained by varying the $\pi \cdots \pi$ distances from 2 Å to 8 Å, Figure 10c. Consequently, the interactions are found to be much more stable in both the dimer's cases accounting for the high through space contributions. Clearly, the 1D potential energy surface of the pyrediylene nanowalls with increased conjugation ($E = -75.4$ kcal mol⁻¹, pyrediylene-2) is found to be 26.8 kcal mol⁻¹ more stable in comparison with the one with the lesser conjugation ($E = -48.6$ kcal mol⁻¹, pyrediylene-1).

Charge Transport Characteristics

Carbon materials show good conducting behaviour due to extended π -conjugation.⁵⁷ To understand the charge career mechanism, we have employed a non-destructive characterization of pyrediylene nanowalls via AC-impedance spectroscopy.⁵⁸ Figure 11a represents the Nyquist plot of bulk pyrediylene in which the real part of the complex impedance (Z') is plotted against its imaginary part ($-Z''$). An equivalent circuit model to understand the Nyquist plot is carried out using the Z-fit program (version 3.2 c). The semicircular behaviour in the fitted plot indicates the Debye behaviour which signifies a single conduction mechanism, where the career hopping mechanism through the conduction channel controls the charge transport.^{58,59} Also, it implies the coexistence of both capacitance and resistance nature of pyrediylene. The capacitance value is estimated to be 1.6×10^{-10} F, exhibiting bulk contribution only. The moderate value of capacitance arises due to the resonance stabilization of highly delocalized charges throughout the highly conjugated framework as inferred from the esp maps (Figure 9a). However, the contributions from the high through bond and through space coupling of π -electrons generate the conduction pathways as

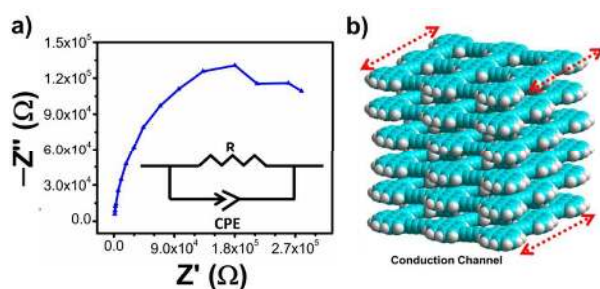


Figure 11. a) Nyquist plot of bulk pyrediyne at 25 °C with equivalent R–C circuit (inset) and b) Hypothetical conduction channel formed via through space interactions of pyrediyne molecules.

shown in Figure 11b resulting in high delocalization of charges within the channel. The electrical conductivity value is estimated to be $\sigma = 1.23(\pm 0.1) \times 10^{-3} \text{ S m}^{-1}$, approximately one order higher than that of graphdiyne ($2.516 \times 10^{-4} \text{ S m}^{-1}$).⁴⁰ Although our preliminary computational results account for an improved electronic structure and intermolecular interactions for the pyrediyne monomer, a full band structure/mobility calculation on such molecules would further extend the scope to derive additional mechanistic insights into the carrier mobilities and electronic structure of this system.^{60,61}

CONCLUSIONS

A new ultrathin, highly planar π -conjugated framework named pyrediyne is synthesized by employing a modified-Glaser-Hay coupling reaction using 1,3,6,8-tetraethynylpyrene as precursor with high scalability, thermal stability and reproducibility. The molecular information is characterized using Raman, XPS, FT-IR, XRD, UV-Vis, FE-SEM, AFM and OM studies. The ultrathin 2D nanowall framework is $\sim 1.4 \text{ nm}$ thick with a lateral size of $\sim 0.6 \mu\text{m}$, where the pyrene units are tethered by diacetylenic linkages to form the π -conjugated network. Thermogravimetric analysis accounted for the excellent thermal stability of the material. TEM images followed by selected area electron diffraction (SAED) pattern along with appearance of several sharp peaks in XRD accounts for the high crystallinity and periodicity of the π -stacked material with significant reflections from a highly ordered BCC lattice structure. Electronic structure information from dispersion corrected DFT calculations suggests high symmetry (C_s point group) and conjugated network of π -electrons accounting for a low band gap of $E_g = 1.17 \text{ eV}$, comparable to that of graphdiyne. As a consequence, the material exhibits an excellent electrical conductivity of $\sigma = 1.23(\pm 0.1) \times 10^{-3} \text{ S m}^{-1}$ as investigated from the electrochemical impedance spectroscopy (EIS) measurements. This value is approximately one order higher than that of graphdiyne ($2.516 \times 10^{-4} \text{ S m}^{-1}$) enabling pyrediyne nanowall as a potential candidate in the field of semiconductor devices and organic electronics such as field effect transistors (FETs), thin film transistors (TFTs) and charge storage applications.

Conflicts of interest

There are no conflicts to declare.

Acknowledgements

We acknowledge departments of chemical engineering and metallurgical-materials engineering at Indian Institute of Technology Madras for the scanning electron microscopy facility. We thank Dr. Balasubramanian Viswanathan, NCCR, IIT Madras for transmission electron microscopy (TEM). We acknowledge Dr. Kothandaraman Ramanujam, department of chemistry, Indian Institute of Technology Madras for providing facilities for EIS measurements. The authors also acknowledge P.G Senapathy Centre for computing resources, IIT Madras for utilizing supercomputing facilities towards DFT calculations performed throughout this work. We acknowledge Department of Chemistry, IIT Madras for all the experimental facilities provided such as Raman, FTIR, XRD, UV-vis, AFM and TGA. P.P and S.S thanks University Grants Commission (UGC), New Delhi, for a fellowship.

References

- Z. Jia, Y. Li, Z. Zuo, H. Liu, C. Huang and Y. Li, *Acc. Chem. Res.*, 2017, **50**, 2470-2478.
- Z. Li, Z. Liu, H. Sun and C. Gao, *Chem. Rev.*, 2015, **115**, 7046-7117.
- N. Lahiri, N. Lotfizadeh, R. Tsuchikawa, V. V. Deshpande and J. Louie, *J. Am. Chem. Soc.*, 2017, **139**, 19-22.
- R. Dong, M. Pfeiffermann, H. Liang, Z. Zheng, X. Zhu, J. Zhang and X. Feng, *Angew. Chem. Int. Ed.*, 2015, **54**, 12058-12063.
- M. Abel, S. Clair, O. Ourdjini, M. Mossoyan and L. Porte, *J. Am. Chem. Soc.*, 2011, **133**, 1203-1205.
- V. Georgakilas, J. A. Perman, J. Tucek and R. Zboril, *Chem. Rev.*, 2015, **115**, 4744-4822.
- Y. Si and E. T. Samulski, *Nano Lett.*, 2008, **8**, 1679-1682.
- S. Kumar, R. Rani, N. Dilbaghi, K. Tankeshwar and K.-H. Kim, *Chem. Soc. Rev.*, 2017, **46**, 158-196.
- F. Wang, D. Kozawa, Y. Miyauchi, K. Hiraoka, S. Mouri, Y. Ohno and K. Matsuda, *Nat. Commun.*, 2015, **6**, 6305/1-6305/7.
- O. Kozak, M. Sudolska, G. Pramanik, P. Cigler, M. Otyepka and R. Zboril, *Chem. Mater.*, 2016, **28**, 4085-4128.
- X. Wei, T. Tanaka, N. Akizuki, Y. Miyauchi, K. Matsuda, M. Ohfuchi and H. Kataura, *J. Phys. Chem. C.*, 2016, **120**, 10705-10710.
- N. Akizuki, S. Aota, S. Mouri, K. Matsuda and Y. Miyauchi, *Nat. Commun.*, 2015, **6**, 8920/1-8920/6.
- D. Zhang, K. Ryu, X. Liu, E. Polikarpov, J. Ly, M. E. Tompson and C. Zhou, *Nano Lett.*, 2006, **6**, 1880-1886.
- C. Doe, H. S. Jang, T. H. Kim, S. R. Kline and S. M. Choi, *J. Am. Chem. Soc.*, 2009, **131**, 16568-16572.
- K. Wang, N. Wang, J. He, Z. Yang, X. Shen and C. Huang, *ACS Appl. Mater. Interfaces*, 2017, **9**, 40604-40613.
- H. Fan and W. Shen, *ChemSusChem.*, 2015, **8**, 2004-2027.
- T. T. Tung, R. Karunakaran, D. N. H. Tran, B. Gao, S. Nag-Chowdhury, I. Pillin, M. Castro, J. F. Feller and D. Losic, *J. Mater. Chem. C.*, 2016, **4**, 3422-3430.
- R. Sakamoto, K. Hoshiko, Q. Liu, T. Yagi, T. Nagayama, S. Kusaka, M. Tsuchiya, Y. Kitagawa, W. Y. Wong and H. Nishihara, *Nat. Commun.*, 2015, **6**, 6713.
- T. Kambe, R. Sakamoto, K. Hoshiko, K. Takada, M. Miyachi, J. H. Ryu, S. Sasaki, J. Kim, K. Nakazato, M. Takata and H. Nishihara, *J. Am. Chem. Soc.*, 2013, **135**, 2462-2465.

ARTICLE

Journal Name

- 20 Y. Wu, P. Qiao, T. Chong and Z. Shen, *Adv. Mater.*, 2002, **14**, 64-67.
- 21 Y. Wu and B. Yang, *Nano Lett.*, 2002, **2**, 355-359.
- 22 Y. Wu, B. Yang, B. Zong, H. Sun, Z. Shen and Y. Feng, *J. Mater. Chem.*, 2004, **14**, 469-477.
- 23 N. Jiang, H. X. Wang, H. Zhang, H. Sasaoka and K. Nishimura, *J. Mater. Chem.*, 2010, **20**, 5070-5073.
- 24 G. Zhao, X. Li, M. Huang, Z. Zhen, Y. Zhong, Q. Chen, X. Zhao, Y. He, R. Hu, T. Yang, R. Zhang, C. Li, J. Kong, J.-B. Xu, R. S. Ruoff and H. Zhu, *Chem. Soc. Rev.*, 2017, **46**, 4417-4449.
- 25 P. Chantharasupawong, C. W. Christenson, R. Philip, L. Zhai, J. Winiarz, M. Yamamoto, L. Tetard, R. R. Nair and J. Thomas, *J. Mater. Chem. C.*, 2014, **2**, 7639-7647.
- 26 N. Zhang, M. Q. Yang, S. Liu, Y. Sun and Y. J. Xu, *Chem. Rev.*, 2015, **115**, 10307-10377.
- 27 P. Mahanandia, F. Simon, G. Heinrich and K. K. Nanda, *Chem. Commun.*, 2014, **50**, 4613-4615.
- 28 X. Yan and L. S. Li, *J. Mater. Chem.*, 2011, **21**, 3295-3300.
- 29 R. K. Joshi, P. Carbone, F. C. Wang, V. G. Kravets, Y. Su, I. V. Grigorieva, H. A. Wu, A. K. Geim and R. R. Nair, *Science*, 2014, **343**, 752-754.
- 30 J. Sun, H. W. Lee, M. Pasta, H. Yuan, G. Zheng, Y. Sun, Y. Li and Y. Cui, *Nanotechnol.*, 2015, **10**, 980-985.
- 31 J. Li, X. Gao, X. Jiang, X.-B. Li, Z. Liu, J. Zhang, C.-H. Tung and L.-Z. Wu, *ACS Catal.*, 2017, **7**, 5209-5213.
- 32 S. Li, Y. Chen, H. Liu, Y. Wang, L. Liu, F. Lv, Y. Li and S. Wang, *Chem. Mater.*, 2017, **29**, 6087-6094.
- 33 C. Wang, P. Yu, S. Guo, L. Mao, H. Liu and Y. Li, *Chem. Commun. (Cambridge, U. K.)*, 2016, **52**, 5629-5632.
- 34 C. Kuang, G. Tang, T. Jiu, H. Yang, H. Liu, B. Li, W. Luo, X. Li, W. Zhang, F. Lu, J. Fang and Y. Li, *Nano Lett.*, 2015, **15**, 2756-2762.
- 35 Y. Xue, J. Li, Z. Xue, Y. Li, H. Liu, D. Li, W. Yang and Y. Li, *ACS Appl. Mater. Interfaces*, 2016, **8**, 31083-31091.
- 36 S. Zhang, H. Liu, C. Huang, G. Cui and Y. Li, *Chem. Commun.*, 2015, **51**, 1834-1837.
- 37 J. Li, X. Gao, B. Liu, Q. Feng, X. B. Li, M. Y. Huang, Z. Liu, J. Zhang, C. H. Tung and L. Z. Wu, *J. Am. Chem. Soc.*, 2016, **138**, 3954-3957.
- 38 S. Zhang, H. Du, J. He, C. Huang, H. Liu, G. Cui and Y. Li, *ACS Appl. Mater. Interfaces*, 2016, **8**, 8467-8473.
- 39 X. Qian, H. Liu, C. Huang, S. Chen, L. Zhang, Y. Li, J. Wang and Y. Li, *Sci. Rep.*, 2015, **5**, 7756/7751-7756/7757.
- 40 G. Li, Y. Li, H. Liu, Y. Guo, Y. Li and D. Zhu, *Chem. Commun.*, 2010, **46**, 3256-3258.
- 41 J. Zhou, X. Gao, R. Liu, Z. Xie, J. Yang, S. Zhang, G. Zhang, H. Liu, Y. Li, J. Zhang and Z. Liu, *J. Am. Chem. Soc.*, 2015, **137**, 7596-7599.
- 42 R. Matsuoka, R. Sakamoto, K. Hoshiko, S. Sasaki, H. Masunaga, K. Nagashio and H. Nishihara, *J. Am. Chem. Soc.*, 2017, **139**, 3145-3152.
- 43 G. Venkataramana and S. Sankararaman, *Eur. J. Org. Chem.*, 2005, **19**, 4162-4166.
- 44 J. A. Pople, *J. Am. Chem. Soc.*, 1980, **102**, 4615-4622.
- 45 S. Ehrlich, J. Moellmann and S. Grimme, *Acc. Chem. Res.*, 2013, **46**, 916-926.
- 46 C. Liu, X. Zhang, L. Li, J. Cui, Y. e. Shi, L. Wang and J. Zhan, *Analyst.*, 2015, **140**, 4668-4675.
- 47 J. Neugebauer, E. J. Baerends, E. V. Efremov, F. Ariese and C. Gooijer, *J. Phys. Chem. A.*, 2005, **109**, 2100-2106.
- 48 E. A. Carrasco F, M. Campos-Vallette, P. Leyton, G. Diaz F, R. E. Clavijo, J. V. Garcia-Ramos, N. Inostroza, C. Domingo, S. Sanchez-Cortes and R. Koch, *J. Phys. Chem. A.*, 2003, **107**, 9611-9619.
- 49 H. Shinohara, Y. Yamakita and K. Ohno, *J. Mol. Struct.*, 1998, **442**, 221-234.
- 50 C. Huang, S. Zhang, H. Liu, Y. Li, G. Cui and Y. Li, *Nano Energy*, 2015, **11**, 481-489.
- 51 H. Ren, H. Shao, L. Zhang, D. Guo, Q. Jin, R. Yu, L. Wang, Y. Li, Y. Wang, H. Zhao and D. Wang, *Adv. Energy Mater.*, 2015, **5** (12), 1500296/1-1500296/6.
- 52 D. Yao, G. Zhang and B. Li, *Nano Lett.*, 2008, **8**, 4557-4561.
- 53 K. Srinivasu and S. K. Ghosh, *J. Phys. Chem. C.*, 2012, **116**, 5951-5956.
- 54 Y. Li, L. Xu, H. Liu and Y. Li, *Chem. Soc. Rev.*, 2014, **43**, 2572-2586.
- 55 G. Luo, X. Qian, H. Liu, R. Qin, J. Zhou, L. Li, Z. Gao, E. Wang, W. N. Mei, J. Lu, Y. Li and S. Nagase, *Phys. Rev. B: Condens. Matter Mater. Phys.*, 2011, **84**, 075439/075431-075439/075435.
- 56 S. Satapathy and E. Prasad, *ACS Appl. Mater. Interfaces*, 2016, **8**, 26176-26189.
- 57 J. Xu, I. Y. Jeon, J. M. Seo, S. Dou, L. Dai and J. B. Baek, *Adv. Mater.*, 2014, **26**, 7317-7323.
- 58 S. Das, P. Chakraborty, A. Shit, S. Mondal and A. K. Nandi, *J. Mater. Chem. A.*, 2016, **4**, 4194-4210.
- 59 S. Das, D. P. Chatterjee and A. K. Nandi, *J. Mater. Chem. A.*, 2014, **2**, 12031-12042.
- 60 M. Long, L. Tang, D. Wang, Y. Li and Z. Shuai, *ACS Nano*, 2011, **5**, 2593-2600.
- 61 S. Pari, A. Cuellar and B. M. Wong, *J. Phys. Chem. C*, 2016, **120**, 18871-18877.